

Extraordinarily transparent compact metallic metamaterials

Samuel J. Palmer,^{1,*} Xiaofei Xiao,^{1,†} Nicolas Pazos-Perez,² Luca Guerrini,² Miguel A. Correa-Duarte,³ Stefan A. Maier,^{1,4} Richard V. Craster,⁵ Ramon A. Alvarez-Puebla,^{2,6} and Vincenzo Giannini⁷

¹*The Blackett Laboratory, Imperial College London, London SW7 2AZ, United Kingdom*

²*Department of Physical Chemistry and EMaS, Universitat Rovira i Virgili, 43007 Tarragona, Spain*

³*Department of Physical Chemistry, Singular Center for Biomedical Research (CINBIO), Southern Galicia Institute of Health Research (IISGS),*

and Biomedical Research Networking Center for Mental Health (CIBERSAM), Universidade de Vigo, 36310 Vigo, Spain

⁴*Nanoinstitut München, Faculty of Physics, Ludwig-Maximilians-Universität München, 80799 München, Germany*

⁵*Department of Mathematics, Imperial College London, London SW7 2AZ, United Kingdom*

⁶*ICREA, Passeig Lluis Companys 23, 08010 Barcelona, Spain*

⁷*Instituto de Estructura de la Materia (IEM-CSIC), Consejo Superior de Investigaciones Científicas, Serrano 121, 28006 Madrid, Spain*

(Dated: November 22, 2018)

Metals are highly opaque, yet we show that densely packed arrays of metallic nanoparticles can be more transparent to infrared radiation than dielectrics such as germanium, even for arrays that are over 75% metal by volume. Despite strong interactions between the metallic particles, these arrays form effective dielectrics that are virtually dispersion-free, making possible the design of optical components that are achromatic over ultra-broadband ranges of wavelengths from a few microns up to millimetres or more. Furthermore, the local refractive indices may be tuned by altering the size, shape, and spacing of the nanoparticles, allowing the design of gradient-index lenses that guide and focus light on the microscale. The electric field is also strongly concentrated in the gaps between the metallic nanoparticles, and the simultaneous focusing and squeezing of the electric field produces strong ‘doubly-enhanced’ hotspots which could boost measurements made using infrared spectroscopy and other non-linear processes over a broad range of frequencies, with minimal heat production.

The future of civilisation will be determined by our ability to create new materials: although no material is truly homogeneous, most materials can be characterised by homogeneous macroscopic properties such as refractive index, which atomistic inhomogeneities smaller than the wavelengths of optical light have been averaged out [1]. Similarly, artificially structured materials known as metamaterials may be described by an effective index, provided that the artificial structuring remains sufficiently subwavelength [2–5].

Early metamaterials included so-called artificial dielectrics, composed of centimeter-scale arrays of metallic particles, that were capable of guiding and focusing radio waves like a dielectric [6]. In contrast to the nanoscale building blocks of modern metamaterials, the metallic particles of early artificial dielectrics were so large compared to the skin depth of the metal that they behaved as perfect conductors and, unsurprisingly, the losses within each particle were negligible such that the arrays were highly transparent to radio waves.

Recently, there has been an interest in building effective dielectrics for the visible and infrared spectrum using nanoscale metallic particle arrays, but the scrutiny of losses has been limited. Chung et al [7] demonstrated that the effective permittivity and permeability of such arrays can be tuned independently, but assumed long wavelengths without considering losses. Soon after this, effective dielectrics with large, tunable effective indexes were realised experimentally [8, 9]. However, the structures in these experiments were not optimised for transparency. Instead, they were only a few layers of nanoparticles thick, such that losses could be largely ignored.

Nevertheless, the underlying physics of the transparency

of densely packed metal metamaterials can be understood by considering how the electrons in metals and dielectrics respond to an electric field (see figure 1). In metals, free electrons are driven to the surfaces until the field generated by the build up of surface charges cancels the applied field within the metal (see figure 1a). On the other hand, the electrons within dielectrics are bound to their parent molecules or atoms (see figure 1b), which polarise in the presence of an electric field [10]. Although the metallic particles comprising the artificial dielectrics possess free electrons, these particles can be regarded as the ‘meta-molecules’ or ‘-atoms’ as the electrons are only free to move within the confines of the metallic particles (see figure 1c), effectively mimicking a dielectric. It is worth noting that this effect is not connected with the creation of plasmonics bands due to the array periodicity [11].

In this work we show that these artificial dielectrics remain highly transparent to infrared radiation even when the particles are nanoscopic such that the electric field penetrates the particles (which can therefore no longer be considered perfect conductors), and when particles are tightly packed such that there are strong interactions between the particles. In fact, we find that these dense arrays of metallic nanoparticles can actually be more transparent than germanium, renowned for its transparency in the infrared, even for arrays exceeding 75% metal by volume. Despite being composed of highly dispersive metals, the effective dielectrics are actually virtually dispersion-free, enabling the design of optical components that are achromatic throughout the mid-to-far-infrared. Furthermore, the local effective index of these components can be tuned by altering the size, shape, and spacing of the

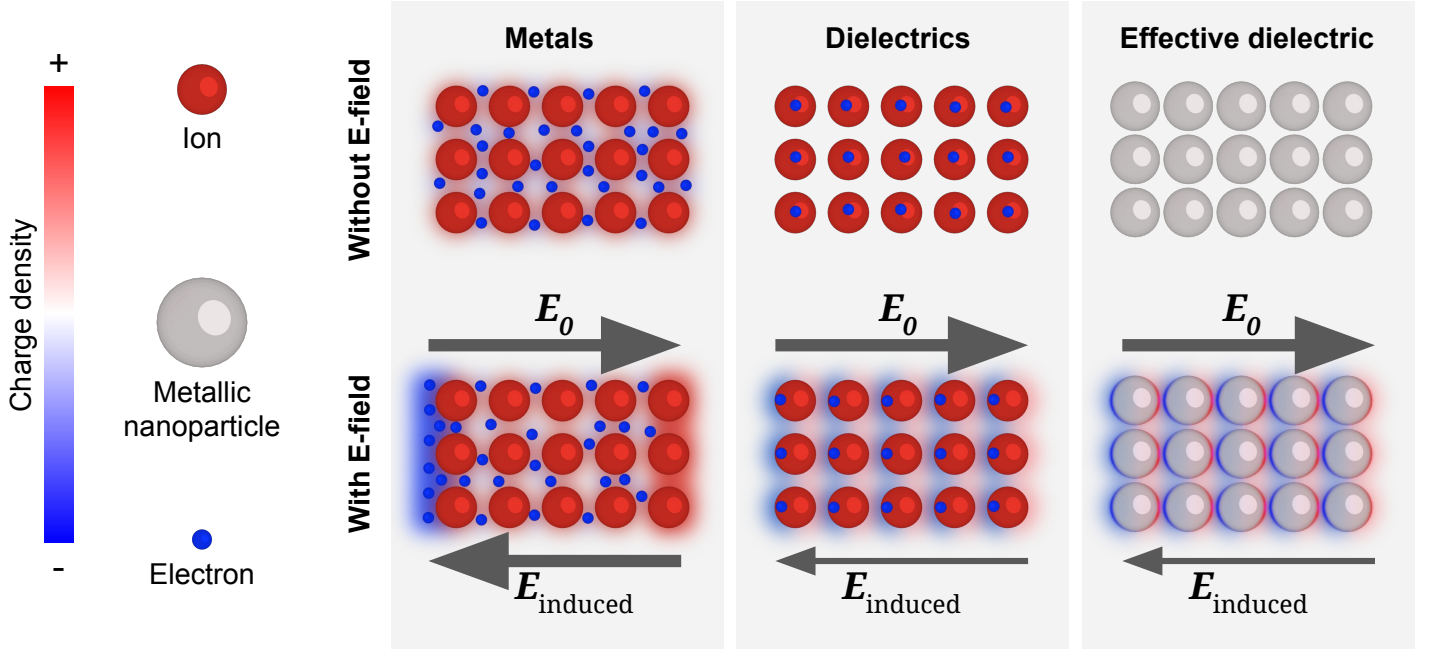


Figure 1. An illustration of how metals, dielectrics, and effective dielectrics respond to a slowly varying electric field. Within in each system, the applied field is opposed by an induced electric field generated by the build up of surface charges. In metals, the electrons are free to move until the applied and induced fields cancel in the bulk. In dielectrics (or effective dielectrics), the surface charge is generated by the polarisation of the (meta-)atoms or (meta-)molecules, and the induced field is weaker than the applied field.

nanoparticles, and is sensitive to the local refractive index of the nanoparticle environment.

Within the array, the electric field is enhanced in the gaps between the metallic nanoparticles. By simultaneously exploiting the transparency, tunability, and high metallic filling fraction of the array, we designed a gradient-index lens that both focuses light on the microscale and ‘squeezes’ the electric field on the nanoscale in order to produce ‘doubly-enhanced’ electric field hotspots, $|E/E_0|^2 > 10^3$, throughout the infrared. We believe that these hotspots could boost measurements made using infrared spectroscopy and other non-linear processes over a broad range of frequencies and with minimal heat production.

Our findings are in contrast to those at optical frequencies, where the excitation of localised surface plasmon resonances (LSPRs) produce a highly dispersive and lossy metallic response, even for filling fractions as low as 1% [12, 13]. When these particles are densely packed, plasmonic coupling produces electric field hotspots [14], but these suffer from the high losses and narrow bandwidths associated with LSPRs [15]. Our results also differ from the case of arrays of dielectric particles with large permittivities, $\epsilon \gg 0$, for which localised ‘magnetic’ plasmon resonances are observed [16].

It can be challenging to calculate the effective index of densely packed arrays of metallic nanoparticles. The components are lossy, highly dispersive, and strongly coupled due to the close packing, and conventional methods such as the plane-wave expansion method would suffer from poor con-

vergence. Additionally, there is a large dissimilarity between the length scales of the large wavelength, small particle, and even smaller gaps which require fine meshing. In traditional methods of solving electromagnetic eigenvalue problems, the frequency, ω , is sought as a function of the permittivity and permeability, ϵ and μ , at a specific position in the Brillouin zone, \mathbf{k} , [17]

$$\omega = \omega(\epsilon(\omega), \mu(\omega), k_x, k_y, k_z). \quad (1)$$

However, this must be solved iteratively as the permittivity and permeability are themselves functions of frequency, which can be particularly problematic for highly dispersive and lossy systems such as ours. Instead of solving for frequency, we solve directly for the Bloch wave vector (see supplementary material),

$$k_z = k_z(\epsilon(\omega), \mu(\omega), k_x, k_y, \omega), \quad (2)$$

from which we may extract the effective index, $n_{\text{eff}} = k_z/k_0$. This allows us to solve for the effective index of compact metallic structures with high accuracy, using finite-differences or finite-elements to discretise our system. Although we solve only for the effective index, we can reasonably assume non-magnetic response $\mu = 1$ for our system at long wavelengths, such that $\epsilon_{\text{eff}} \approx n_{\text{eff}}^2$. It will be seen that there is good agreement between simulations assuming no magnetic response and high resolution simulations of the full geometry.

In figure 2, we contrast the transparency of arrays of nanocylinders and nanospheres to germanium, although in

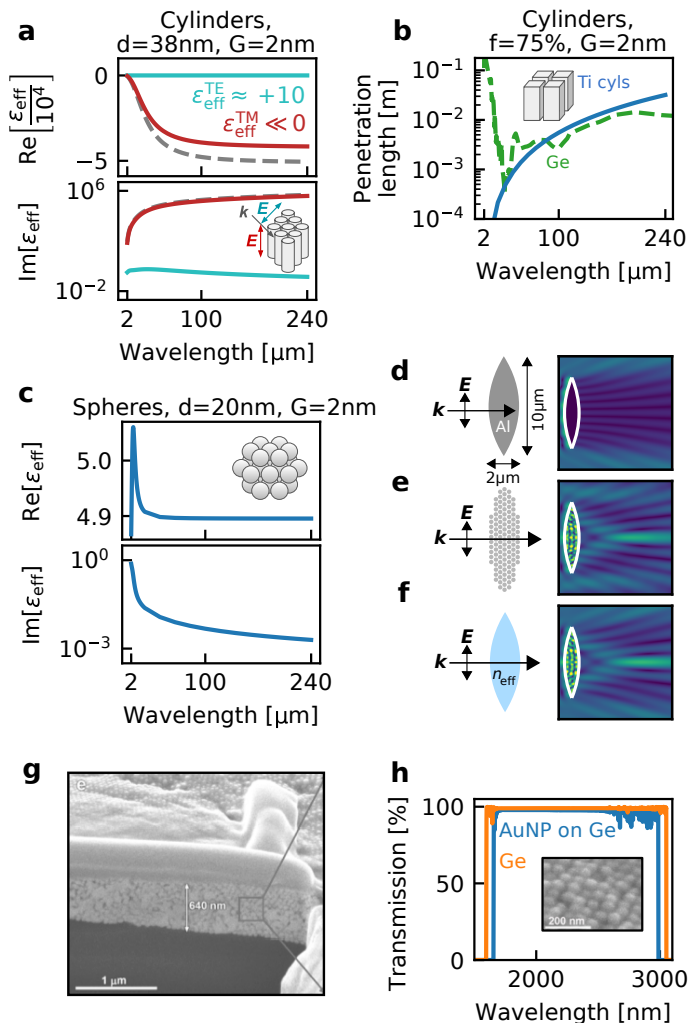


Figure 2. (a) The effective permittivity of an array of aluminium nanocylinders for TE (blue curve) and TM (red curve) polarised light compared to the permittivity of solid aluminium (dashed curve). (b) The effective penetration length of the nanoparticle arrays can exceed that of real dielectrics, such as germanium, even for metallic filling fractions as high as 75%. (c) The effective permittivity of titanium nanospheres for unpolarised light. (d-f) The arrays of nanoparticles are transparent enough to act as micrometer-scale lenses to infrared radiation of wavelength $\lambda_0 = 2 \mu\text{m}$, as shown by the magnetic near-fields. There is good agreement between (e) the full geometry of aluminium cylinders with diameter 38 nm and surface-to-surface gap 2 nm and (f) the homogenised geometry, $n_{\text{eff}} = 3.2 + 0.05i$. (g) Microscopy image of 60 nm diameter gold colloidal supercrystal deposited on a Ge substrate that shows high infrared transparency (h).

principle the nanoparticles could have other shapes, and demonstrate that these arrays can guide and focus light. Figure 2a shows that arrays of nanocylinders behave as effective dielectrics ($\epsilon_{\text{eff}} > 0$) for transverse electric polarised light (TE, blue line). This is because a transverse force on the electrons leads to oscillating surface charges that mimic the oscillating dipoles of an atom (or molecule) in a real dielec-

tric. In contrast, the response of the cylinders to transverse magnetic polarised light (TM, red line) is similar to the response of the bulk metal (grey dashes) as the electrons are free to move under the action of the longitudinal electric field without encountering the surfaces of the cylinders.

Remarkably, these arrays can be more transparent than real dielectrics such as germanium, even when the system is over 75% metal as in figure 2b. Furthermore, it is shown in figure 2c that arrays of nanospheres behave as effective dielectrics regardless of the incident polarisation, as the forcing of electrons in any direction results in surface charges that imitate the oscillating dipoles of a dielectric.

Our effective index calculations were validated using finite-difference time-domain simulations of a plane wave, $\lambda_0 = 2 \mu\text{m}$, impinging on a primitive lens shape from the left-hand side. As expected, there is no transmission through the solid aluminium in figure 2d because aluminium has a skin depth of about 10 nm at this wavelength, which is much smaller than the lens thickness of $2 \mu\text{m}$. The observed fringes in intensity are in fact caused by diffraction around the lens. However, breaking the solid aluminium into an array of aluminium nanocylinders, as in figure 2e, produces a transparent lens capable of focusing light which closely resembles the behaviour of the homogeneous dielectric lens of figure 2f, despite consisting of 82% metal by volume.

To test the accuracy of the proposed theory, a highly ordered colloidal supercrystal [18] was produced with gold nanoparticles of diameter 60 nm (see supplementary material). The supercrystal was deposited on a germanium window (figure 2g) and characterized in a UV-Vis-NIR spectrophotometer (figure 2h). Notably, the material shows an outstanding transparency until 3000 cm^{-1} (detector cut off), demonstrating the feasibility of experimental production of the suggested materials.

As a continuation (see figure 3) we investigate how the effective index and losses are modified by the skin depth, $\delta_s = \lambda_0/4\pi\kappa$, defined as the distance the field penetrates into a metal before the intensity decays by a factor of $1/e$. As shown in the inset of figure 3a, different metals have different skin depths, but for Drude metals the skin depth generally increases with wavelength as $\delta_s \sim \sqrt{\lambda}$ throughout the infrared. We observe that metals with longer skin depths produce the most transparent and least dispersive nanoparticle arrays. We also note that at long wavelengths the effective index of each array is tending to the same value for all four metals.

Successively (figure 3b), we compare our results to the Maxwell Garnett (MG) mixing formula [20], in which sub-wavelength particles are approximated as non-interacting dipoles, and the polarisability of each dipole is taken as the quasi-electrostatic polarisability of the corresponding particle. In principle, this approximation should fail at high filling fractions due to non-dipolar contributions at the small gaps [21–24], but nonetheless remains surprisingly accurate for the filling fractions used here. For cylindrical particles in air or

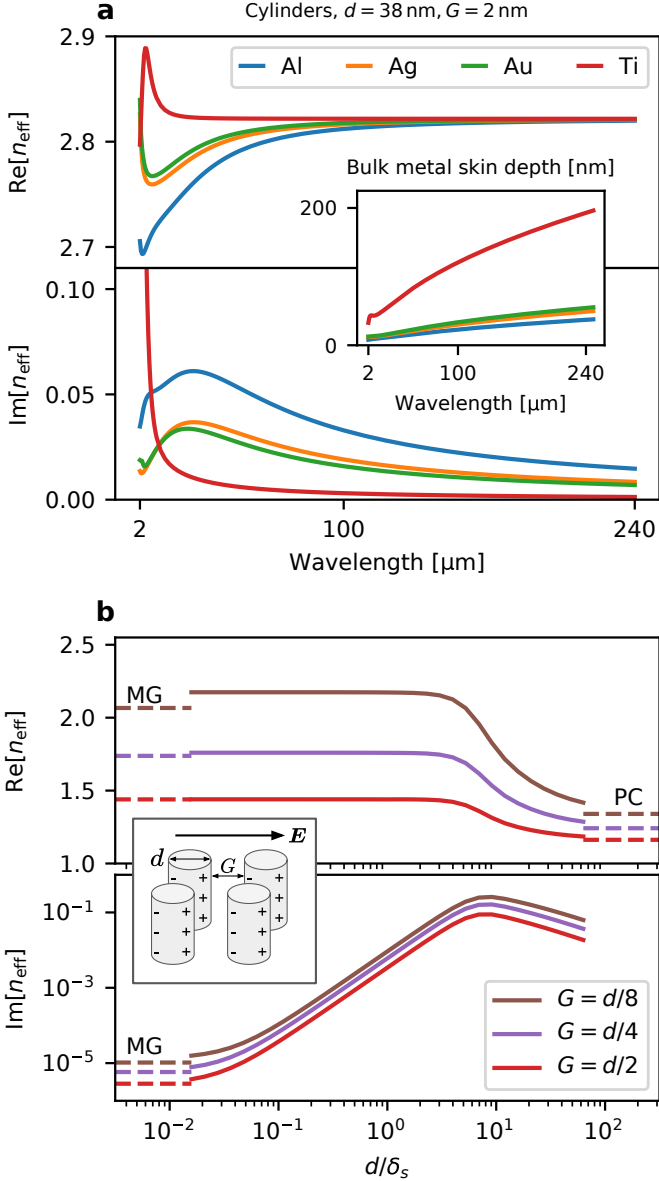


Figure 3. (a) The effective index of a square array of nanocylinders, composed of aluminium, gold, silver, and titanium. Inset: the skin depth of each metal, calculated using the Lorentz-Drude model of permittivity with data from Rakic et al [19]. (b) The ratio of the particle diameter to the skin depth of the metal determines whether the particles behave as quasi-static dipoles or perfect conductors. The effective index is remarkably constant for $\delta_s \gtrsim d$.

vacuum, the MG mixing formula reads

$$\epsilon_{\text{MG}}^{\text{cyl}} = \frac{\epsilon + 1 + f(\epsilon - 1)}{\epsilon + 1 - f(\epsilon - 1)}, \quad (3)$$

where ϵ and f are the permittivity and filling fraction of the cylinders, respectively. When $|\epsilon| \gg 1$, as with Drude metals

at long wavelengths, the MG mixing formula tends to

$$\epsilon_{\text{MG}}^{\text{cyl}} \approx \frac{1 + f}{1 - f} - \frac{4f}{(1 - f)^2} \frac{1}{\epsilon} + \mathcal{O}\left(\frac{1}{\epsilon^2}\right), \quad (4)$$

which is, to first order, both real and independent of the permittivity.

As expected, the effective index is well approximated by the MG mixing formula when the filling fraction is low and the particle is small compared to the skin depth. As the size of the particle is increased relative to the skin depth, the system diverges from the quasi-electrostatic limit and, at first, the losses rise as electromagnetic field is retarded. However, when the particles become much larger than the skin depth, the losses begin to fall again as the metal behaviour transitions to that of a perfect conductor (PC, dashes of figure 3b).

At high filling fractions, the MG mixing formula underestimates the effective index of the array. This is because MG neglects the attractive forces between neighbouring surface charges (see figure 3b inset) which increase the effective polarisability of the particles.

In addition to being highly transparent, the system is highly tunable by controlling the size, shape, and spacing of the particles. In figure 4a, we demonstrate that we can tune an anisotropic response by controlling the aspect ratio of arrays of elliptical cylinders. We compare our numerical method (solid lines) and the corresponding MG mixing formula (dashes, see supplementary material),

$$\epsilon_{\text{MG}}^{\text{ell-cyl}} = \frac{\epsilon + \Lambda + \Lambda f(\epsilon - 1)}{\epsilon + \Lambda - f(\epsilon - 1)}, \quad (5)$$

where $\Lambda = \sqrt{L_{\parallel}/L_{\perp}}$ is the aspect ratio of the cylinder, and L_{\parallel} and L_{\perp} are the elliptical axes of the cylinder parallel and perpendicular to the electric field, respectively.

The numerical results demonstrate that we can easily tune the effective index to vary by up to 25% as the system is rotated. The geometry, shown in the insets of figure 4a, was constructed by distorting square arrays of circular cylinders.

For the real part of n_{eff} , there is general agreement between our numerics and the MG mixing formula. However, note that for extreme aspect ratios, $L_{\parallel}/L_{\perp} \ll 1$ or $L_{\parallel}/L_{\perp} \gg 1$, the real part of n_{eff} is over- and underestimated, respectively, by the MG mixing formula. From consideration of the geometry figure 4a, we believe that this is because interactions between horizontally adjacent particles are enhanced for small aspect ratios, whereas for large aspect ratios it is the interactions between vertically adjacent particles that are enhanced. Since the incident electric field is horizontally polarised, each particle acts as a horizontally aligned dipole, and the effective polarisability of the array is increased by horizontal interparticle interactions and decreased by vertical interparticle interactions.

The true losses of the distorted array are higher than those predicted by MG, for the same reasons as discussed in figure 3c, but are still much lower than for bulk metal. Interestingly, the losses are lower for the distorted arrays as the retardation effects are lessened when the particles are thin.

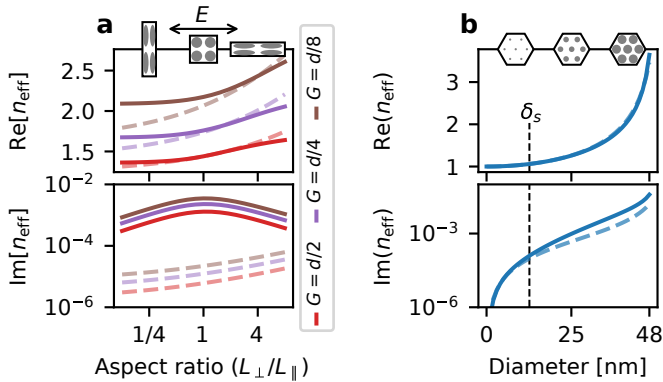


Figure 4. The effective index of gold nanocylinders as functions of aspect ratio and particle size, calculated numerically (solid lines) and with the Maxwell Garnett mixing formula (dashes). (a) The aspect ratios of square arrays of cylinders were varied, while keeping the volume of each cylinder and the filling fraction of the array constant, as shown in the insets. The incident wavelength was $\lambda_0 = 200 \mu\text{m}$. (b) The cylinders were placed on a triangular lattice of length 50 nm , and their diameters were varied from $0 \text{ nm} \leq d \leq 48 \text{ nm}$ for an incident wavelength of $\lambda_0 = 2 \mu\text{m}$.

The effective index can also be tuned by fixing the particle positions and tuning their sizes. In figure 4b, the agreement between the numerics (solid line) and MG (dashes) was surprisingly good, even when $d > \delta_s$, although losses were noticeably increased for diameters larger than the skin depth.

To highlight our ability to tune the local effective index, we constructed a gradient-index (GRIN) lens using the same triangular lattice of gold cylinders that was studied in figure 4b, but varying the diameters of the cylinders with position. The schematic of the lens is shown in figure 5a. By using the GRIN lens to simultaneously focus light on the microscale and ‘squeeze’ light on the nanoscale, we were able to produce intense, ‘doubly-enhanced’ electric field hotspots. Unlike plasmonic enhancements, this effect is not based on lossy resonances and is both broadband and low-loss.

In order to maximise the squeezing of the electric field, the focal point of the GRIN lens must coincide with the region of closest packing. For this reason, we chose the so-called ‘concentrator’ lens, $n_{\text{eff}}^{\text{conc}}(r) = R/r$, the focal point of which is located at the origin [25].

The cylinder diameters varied slowly enough that figure 4b could still be used to determine the diameter necessary to achieve a given local effective index. In mapping from effective index to cylinder diameter, it was necessary to truncate the effective index of the lens at $n_{\text{eff}} \approx 3.5$, as shown in figure 5b. This reduced the quality of the focus, but was sufficient for our purposes.

We can see from the magnetic near-fields in figure 5c that the performance of the cylinders designed and tuned in this manner agrees well with the targeted effective lens behaviour. Although the lens was tuned to operate at a wavelength of $2 \mu\text{m}$, the dispersion of the metamaterial is low for all wavelengths $\lambda_0 \gtrsim 2 \mu\text{m}$, and we see that the lens performs equally

well at larger wavelengths, such as $\lambda_0 = 5 \mu\text{m}$.

Unlike the magnetic field, which is continuous across the air-metal interfaces, the electric field is strongly localised in the gaps as shown in figure 5d. This squeezing of a $2 \mu\text{m}$ wavelength into 2 nm gaps combined with the focusing effects of the lens produced strong hotspots of intensity $|E/E_0|^2 > 10^3$. We believe that these hotspots could be used to enhance non-linear processes, such as infrared spectroscopy, over a much broader range of wavelengths than could be achieved with resonance-based enhancements.

In conclusion, low-loss effective dielectrics can be constructed from arrays of metallic nanoparticles. These arrays are highly transparent, at times even exceeding the transparency of real dielectrics renowned for their transparency to low energy radiation, such as germanium, and can be tuned locally by controlling the size, shape, and spacing of the particles. Furthermore, and in contrast to metamaterials designed upon resonant effects, the effective index is essentially constant for all wavelengths greater than about $2 \mu\text{m}$. This allows the design of optical devices to guide or enhance light over an extremely broad range of frequencies, essentially without an upper bound on wavelength.

ACKNOWLEDGEMENTS

Ramon A. Alvarez-Puebla thanks the MINECO-Spain (CTM2014-58481R, CTM2017-84050R, CTQ2017-88648R, RYC-2015-19107 and RYC2016-20331), Xunta de Galicia (Centro Singular de Investigacion de Galicia, Acc. 2016-19 and EM2014/035), Generalitat de Catalunya (2017SGR883), URV (2017PFR-URV_B2-02), URV and Banco Santander (2017EXIT-08) and European Union (ERDF). Xiaofei Xiao acknowledges the Lee Family Scholarship. Stefan Maier and Richard Craster acknowledge the EPSRC Mathematical Fundamentals of Metamaterials programme grant (EP/L024926/1), and Stefan Maier additionally acknowledges the Lee-Lucas Chair in Physics.

Thanks to Rodrigo Berte and Ory Schnitzer for the stimulating discussions.

* samuel.palmer12@imperial.ac.uk

† xiaofei.xiao15@imperial.ac.uk

- [1] JD Jackson. Classical electrodynamics, 1999.
- [2] JB Pendry, AJ Holden, WJ Stewart, and I Youngs. Extremely low frequency plasmons in metallic mesostructures. *Physical review letters*, 76(25):4773, 1996.
- [3] JB Pendry, AJ Holden, DJ Robbins, and WJ Stewart. Magnetism from conductors and enhanced nonlinear phenomena. *IEEE transactions on microwave theory and techniques*, 47(11):2075–2084, 1999.
- [4] DR Smith, JB Pendry, and MCK Wiltshire. Metamaterials and negative refractive index. *Science*, 305(5685):788–792, 2004.
- [5] W Cai and VM Shalae. Optical metamaterials, vol. 10, 2010.

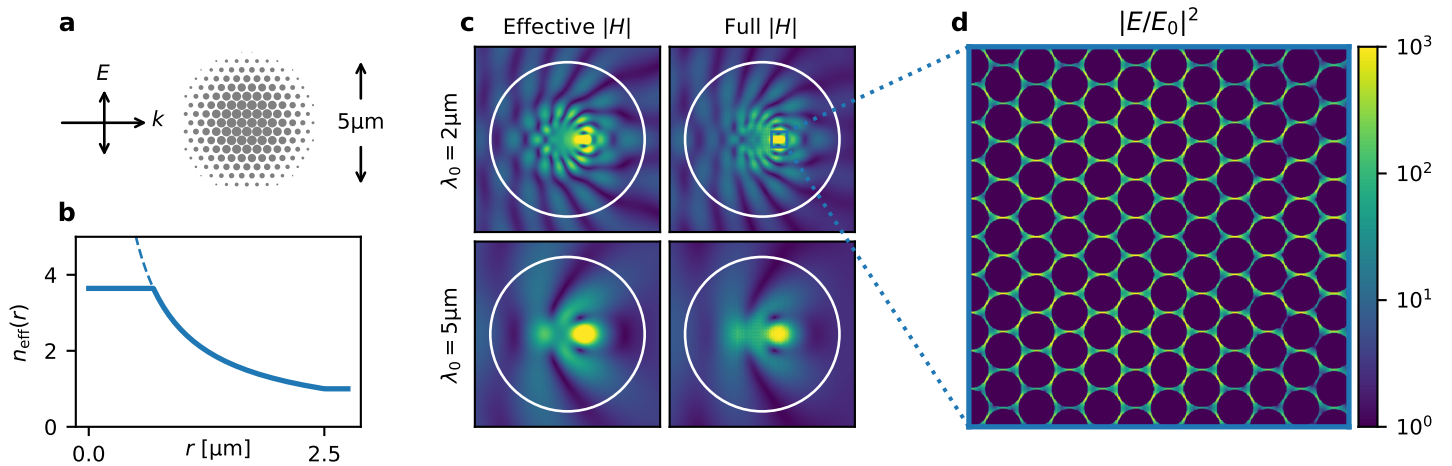


Figure 5. (a) Schematic of a ‘concentrator’ gradient-index lens composed of gold nanocylinders on a triangular lattice with 50 nm site-to-site separation. (b) Effective index profile of the concentrator lens, ideal (dashed) and achieved (solid). (c) Magnetic near-fields calculated using the effective geometry and the full geometry both confirm that plane waves are focused towards the origin of the lens. (d) Within the focal point of the lens, the combined focusing and squeezing of the electric field produces ‘doubly-enhanced’ hotspots.

- [6] WE Kock. Metallic delay lenses. *Bell Labs Technical Journal*, 27(1):58–82, 1948.
- [7] K Chung, R Kim, T Chang, and J Shin. Optical effective media with independent control of permittivity and permeability based on conductive particles. *Applied Physics Letters*, 109(2):021114, 2016.
- [8] D Doyle, N Charipar, C Argyropoulos, SA Trammell, R Nita, J Naciri, A Pique, JB Herzog, and J Fontana. Tunable subnanometer gap plasmonic metasurfaces. *ACS Photonics*, 5(3):1012–1018, 2017.
- [9] R Kim, K Chung, JY Kim, Y Nam, SK Park, and J Shin. Metal nanoparticle array as a tunable refractive index material over broad visible and infrared wavelengths. *ACS Photonics*, 5(4):1188–1195, 2018.
- [10] DR Frankl. *Electromagnetic theory*. Prentice Hall, 1986.
- [11] JG Rivas, G Vecchi, and V Giannini. Surface plasmon polariton-mediated enhancement of the emission of dye molecules on metallic gratings. *New Journal of Physics*, 10(10):105007, 2008.
- [12] MB Ross, MG Blaber, and GC Schatz. Using nanoscale and mesoscale anisotropy to engineer the optical response of three-dimensional plasmonic metamaterials. *Nature Communications*, 5:4090, 2014.
- [13] MB Ross, CA Mirkin, and GC Schatz. Optical properties of one-, two-, and three-dimensional arrays of plasmonic nanostructures. *The Journal of Physical Chemistry C*, 120(2):816–830, 2016.
- [14] V Mondes, E Antonsson, J Plenge, C Raschpichler, I Halfpap, A Menski, C Graf, MF Kling, and E Rühl. Plasmonic electric near-field enhancement in self-organized gold nanoparticles in macroscopic arrays. *Applied Physics B*, 122(6):155, 2016.
- [15] SA Maier. *Plasmonics: fundamentals and applications*. Springer Science & Business Media, 2007.
- [16] R Paniagua-Domínguez, LS Froufe-Pérez, JJ Sáenz, and JA Sánchez-Gil. Localized magnetic plasmons in all-dielectric $\mu < 0$ metastructures. *Physical Review B*, 91(23):235120, 2015.
- [17] JD Joannopoulos, SG Johnson, JN Winn, and RD Meade. *Photonic crystals: molding the flow of light*. Princeton University Press, 2011.
- [18] M Tebbe, S Lentz, L Guerrini, A Feryc, RA Alvarez-Puebla, and N Pazos-Perez. Fabrication and optical enhancing properties of discrete supercrystals. *Nanoscale*, 8:12702–12709, 2016.
- [19] AD Rakić, AB Djurišić, JM Elazar, and ML Majewski. Optical properties of metallic films for vertical-cavity optoelectronic devices. *Applied optics*, 37(22):5271–5283, 1998.
- [20] CF Bohren and DR Huffman. *Absorption and scattering of light by small particles*. John Wiley & Sons, 2008.
- [21] A Alù. First-principles homogenization theory for periodic metamaterials. *Physical Review B*, 84(7):075153, 2011.
- [22] A Alù, AD Yaghjian, RA Shore, and MG Silveirinha. Causality relations in the homogenization of metamaterials. *Physical Review B*, 84(5):054305, 2011.
- [23] XX Liu and A Alù. Generalized retrieval method for metamaterial constitutive parameters based on a physically driven homogenization approach. *Physical Review B*, 87(23):235136, 2013.
- [24] DR Abujetas, R Paniagua-Domínguez, M Nieto-Vesperinas, and JA Sánchez-Gil. Photonic band structure and effective medium properties of doubly-resonant core-shell metallo-dielectric nanowire arrays: low-loss, isotropic optical negative-index behavior. *Journal of Optics*, 17(12):125104, 2015.
- [25] A Climente, D Torrent, and J Sánchez-Dehesa. Gradient index lenses for flexural waves based on thickness variations. *Applied Physics Letters*, 105(6):064101, 2014.